

Direct cortical control of muscle activation in voluntary arm movements: a model

Emanuel Todorov

Gatsby Computational Neuroscience Unit, University College London, 17 Queen Square London WC1N 3 AR, UK

Correspondence should be directed to E.T. (emo@gatsby.ucl.ac.uk)

What neural activity in motor cortex represents and how it controls ongoing movement remain unclear. Suggestions that cortex generates low-level muscle control are discredited by correlations with higher-level parameters of hand movement, but no coherent alternative exists. I argue that the view of low-level control is in principle correct, and that seeming contradictions result from overlooking known properties of the motor periphery. Assuming direct motor cortical activation of muscle groups and taking into account the state dependence of muscle-force production and multi-joint mechanics, I show that cortical population output must correlate with hand kinematics in quantitative agreement with experimental observations. The model reinterprets the 'neural population vector' to afford unified control of posture, movement and force production.

Since electrical stimulation of a region of cortex was discovered to evoke movement a century ago, the debate about the 'level' of movement control exerted by primary motor cortex (MI) continued¹. Its crucial role in the production of all voluntary arm movements is evidenced by the almost complete paralysis following MI lesions². Studies in awake behaving monkeys seem to establish that the activity of most MI pyramidal tract neurons is directly related to the amount of force exerted³. Such an involvement in low-level muscle control is consistent with the dense projection from MI to the spinal cord⁴ (often directly onto motor neurons), and with linkage of corticomotor neuronal firing with muscle activity, as revealed by spike-triggered averaging⁵.

This view is challenged by the observation that the MI population encodes both the direction⁶ and magnitude^{7,8} of movement velocity—cells encoding force should fire in relation to acceleration, not velocity. Yet the same cells that encode hand velocity in movement tasks can also encode the forces exerted against external objects in both movement and isometric tasks^{9,10}. To complicate matters further, MI firing was also correlated with arm position¹¹, acceleration¹², movement preparation¹³, target position¹⁴, distance to target¹⁵, overall trajectory¹⁶, muscle coactivation¹⁷, serial order¹⁸, visual target position¹⁹ and joint configuration²⁰. In addition, the nature of the MI encoding seemed to vary systematically within each trial—with instantaneous movement curvature⁷ or time from movement onset¹⁵.

This plethora of correlations, previously summarized by the statement, "... all types of neuron that were looked for were found, in nearly equal numbers"¹³, casts serious doubt on a low-level muscle-control theory of MI. However, there is no proposed alternative that is satisfying and equally simple. At one extreme, we have descriptive regression models^{15,21} implying that MI neurons control every movement parameter that correlates significantly with their firing. Although these models can fit the data well, they leave a crucial question unanswered, namely, how such a mixed signal can be useful for generating motor behavior. The

problem is that most of the proposed movement parameters are related through the laws of physics, and therefore the spinal circuitry cannot control them independently even if it somehow managed to decode the mixed MI signal in real time. The other extreme is to question whether "movement parameters are recognizably coded in the activity of single neurons" in the first place²². It is argued that they are not and do not need to be, as all that matters is the population average of the descending projections²². However it should still be possible to understand the average population activity, if not the firing of individual neurons. Yet a number of the above observations made on the population level conflict with one another.

My model assumes that each pyramidal tract neuron contributes additively, either via direct projections onto motor neurons or indirectly through spinal interneurons, to the activation of a muscle group⁵ (see Methods). Thus muscle activity (motor neuron firing) simply reflects the firing in MI. How can such a model explain the numerous correlations with endpoint kinematic parameters? The basic idea is the following: these correlations are puzzling only if one assumes that muscle activation is identical to endpoint force. But that assumption is incorrect—muscle force depends not only on activation, but also on muscle length and rate of change of length^{23–25}. Thus, to produce a certain endpoint force, the MI output has to compensate for the muscle's state dependence (as well as effects of multi-joint mechanics). This position-and velocity-dependent compensation (a kinematic signal) gives rise to a number of correlations between MI firing and endpoint kinematics, which, taken at face value, imply a much higher level of MI control than is necessary to explain them.

In contrast with descriptive models that merely fit the data, my model is mechanistic: it first postulates how MI activity causes motor behavior, and then explains the observed correlations as emergent properties of that causal flow. Note that mechanistic models are more commonly used to explain their outputs given

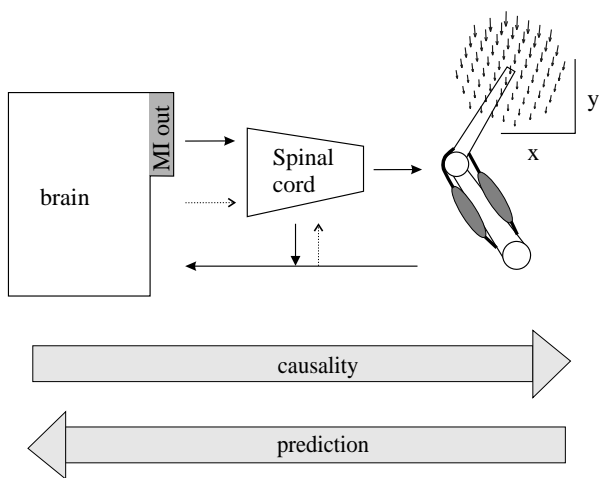
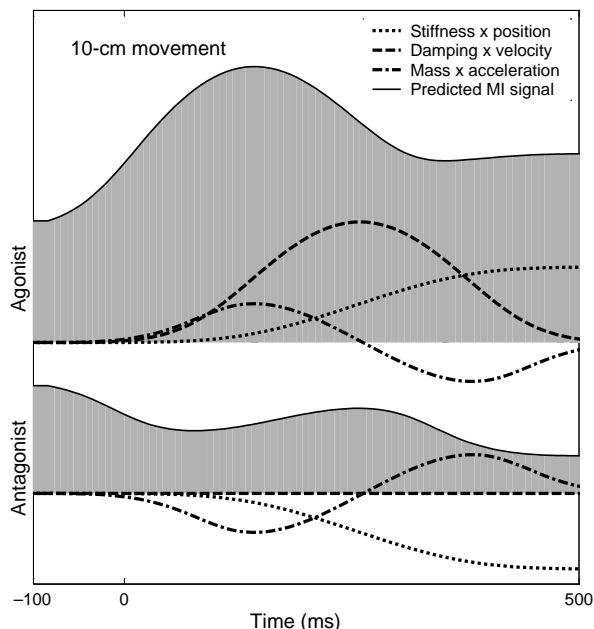


Fig. 1. Mechanistic model of the motor periphery. The ‘brain’ receives sensory feedback, combines it with motor plans, and somehow ‘decides’ what to do next. The focus of the model is the causal flow from the MI output through spinal processing, muscle force production and multi-joint mechanics to endpoint force. Predictions about MI activity are obtained by ‘inverting’ that causal flow. Pathways corresponding to light arrows are ignored (but see Discussion). The illustrated position-dependent force field corresponds to an elbow flexor with fixed moment arm, acting around a planar 2-link arm with link lengths of 30 cm (not drawn to scale) over a 20 cm × 20 cm workspace. Note that direction varies little, and forces become smaller (because of muscle shortening) for displacements in the force direction. Such force fields will be modeled as parallel over the workspace of interest.

the inputs²⁶. For a model of the motor periphery the situation is reversed (Fig. 1). The output (motor behavior) specified by the motor task is easily measured, and the input (MI firing) must be explained. This introduces a complication: the causal flow from MI firing to net endpoint force is a many-to-one mapping, and thus, is not invertible. Because there exists a large ‘null-space’ of MI firing patterns that all give rise to the same net force, the



model cannot predict the activities of individual MI neurons. It can only predict that the observed MI firing will be constrained to the null-space corresponding to the observed endpoint force. This prediction takes the form of a population average, equivalent to the ‘population vector’ routinely computed in the experimental literature⁶.

RESULTS

Constraints on MI activity

I assume delayed linear summation of MI outputs, a first-order model of muscle force production, and a local linear approximation to multijoint kinematics over a small workspace. The impedance of the four-degree-of-freedom arm, muscle forces and movement kinematics are all expressed in two-dimensional endpoint space. The derivation in Methods yields the following result: the vector $c(t - \Delta)$ of instantaneous MI outputs at time $t - \Delta$, multiplied by the matrix of a cell’s endpoint-force directions, has to satisfy (up to an arbitrary scaling factor)

$$Uc(t - \Delta) = F^T f(t) + m\ddot{x}(t) + b\dot{x}(t) + kx(t) \quad (1)$$

Average endpoint inertia, viscosity and damping are given by m , b and k , $x(t)$ is the two-dimensional hand position at time t , and $F_{2 \times 2}$ is a matrix encoding the anisotropy of the Jacobian. (The Jacobian is the matrix of derivatives of endpoint coordinates with respect to joint angles.)

Equation 1 is the constraint mentioned above on the MI activation pattern $c(t - \Delta)$ corresponding to motor behavior $f(t)$, $\dot{x}(t)$, $\ddot{x}(t)$, $x(t)$. It is the starting point for all results presented below. Importantly, the activity of individual muscles was ‘integrated out’ (see Methods) so that the constraint on MI firing is expressed in endpoint space and depends only on behavioral parameters and arm impedance. The model has only four parameters—the scalars m , b and k and the aspect ratio of F —which all can be inferred from the literature (details in Methods and Fig. 2). Throughout the paper they are fixed to $m = 1$ kg, $b = 10$ N·s/m, $k = 50$ N/m, approximate values for the human arm. Scaling down all parameters does not affect the model.

To address experimental descriptions of individual cell firing, equation 1 is augmented with the assumption of cosine tuning⁶ (and identical preferred directions) for force, velocity and displacement^{9,11,27}. I show elsewhere that cosine tuning is the only activation profile that minimizes neuromotor noise—which makes it a principled choice. A sketch of that argument is given in Methods. Taking into account the asymmetry of muscle damping, the activation of cell c_i with force direction u_i is

$$c_i(t - \Delta) = C + \frac{u_i^T}{2} (F^T f(t) + m\ddot{x}(t) + kx(t)) + b[u_i^T \dot{x}(t)] \quad (2)$$

Fig. 2. Composition of the MI signal, showing the signals for a 10-cm, 500-ms straight movement with a bell-shaped speed profile. The difference between agonist and antagonist activation is due to asymmetric damping, which is present only for muscle shortening (that is, in the agonist direction). Neural activity is advanced by $\Delta = 100$ ms throughout the paper. In all simulations $m = 1$ kg, $b = 10$ N·s/m, $k = 50$ N/m. The terms m and b are proportional to perturbation estimates for the human arm³¹, k is about 50% smaller for two reasons. Perturbation experiments measure combined effects of intrinsic muscle stiffness (which the model compensates for) and reflex contributions—in deafferented patients, stiffness is about 50% smaller⁴⁹. More importantly, the slope of the isometric length-tension curve is much smaller than muscle stiffness measured via artificial, abrupt stretch²³ (presumably because of elasticity of crossbridges).

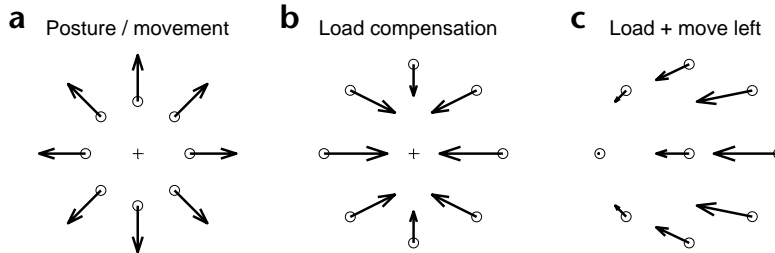


Fig. 3. Predicted population vectors. The origin (\circ) of each PV corresponds to the direction of movement/load relative to the center of the workspace (+). The movement PV is the average over the movement time: $\int_0^T (m\ddot{x}(t) + b\dot{x}(t) + kx(t))dt$. The posture PV is the value at the end of the trial: $kx(T)$. The load compensation PV is the value before movement: $F^{-1}f(0)$. The combined movement + load PV is: $\int_0^T (F^{-1}f(t) + m\ddot{x}(t) b\dot{x}(t) + kx(t))dt$. The scale of the plots is arbitrary. The movement kinematics is given in Fig. 2. (a) The PV for movement/posture is symmetric. (b) Distortions of load PV result from the anisotropy of the F matrix (f opposes the external load and thus, the reversed direction). (c) Center movement to the left, no load. The eight surrounding clusters correspond to a movement to the left in the presence of three-newton loads in each of eight directions. The load magnitude is bigger than that used experimentally⁹ because the impedance parameters here are also greater than those for a monkey arm.

It can be verified that the c_i s given by equation 2 satisfy equation 1 under a uniform distribution of force directions. Note that $u^T x$ is the dot-product of vectors u and x , which is proportional to the cosine of the angle between them. The constant C can be thought of as a baseline or cocontraction command (specified independently).

Apparent velocity encoding

In the one-dimensional case, the quantity U_C is simply the difference between agonist (A) and antagonist (N) activity: $c_A - c_N = f(t)/F + m\ddot{x}(t) + b\dot{x}(t) + kx(t)$. How is that quantity distributed between c_A and c_N ? The simplest possibility is that it is divided equally, except for the asymmetric damping term which affects only muscles pulling in the direction of movement. Thus

$$\begin{aligned} c_A(t - \Delta) &= C + \frac{1}{2}(f(t)/F + m\ddot{x}(t) + kx(t)) + b\dot{x}(t) \\ c_N(t - \Delta) &= C - \frac{1}{2}(f(t)/F + m\ddot{x}(t) + kx(t)) \end{aligned} \quad (3)$$

During isometric force production, the only time-varying term is $f(t)$; thus the population seems to encode the magnitude of muscle force^{3,5}. Now consider the activity of the same population during movement (Fig. 2). The crucial point is that, for hand kinematics in the physiological range with an experimentally measured inertia-to-damping ratio, the damping compensation signal actually dominates the acceleration signal. Thus the population activity resembles the velocity profile^{7,8,27}, although the cells directly control muscle activation. Note also the asymmetry between agonist and antagonist activity, which, in the model, is a natural consequence of muscle damping asymmetry. Although the latter effect is clear from several data sets^{8,9,27}, it is rarely commented upon.

Reinterpretation of the population vector

The lines of action of facilitated muscles overlap with the cell's physiological preferred direction (PD)⁵. To the extent that this also holds in the multijoint case, the neural population vector

(PV), defined as the vector sum of PDs scaled by cell activations⁶, is identical to the left-hand side of equation 1 ($U_C = \sum c_i u_i$). In other words, the model predicts that the population vector, as commonly defined in the MI literature, is equal not to the movement direction or velocity^{6,7}, but instead to the particular sum of position, velocity, acceleration and force signals in equation 1. Additivity of movement and load-related signals is observed experimentally⁹.

The predicted PV, the vector corresponding to the right-hand side of equation 1, for movement, posture, external-load compensation and movement with variable loads (Fig. 3) are in close agreement with existing data. The PV reconstructs the movement direction well^{6,9}, but the reconstruction of load direction is distorted⁹, and the reconstruction fails when both movement and load direction are varied independently²⁸.

The difference between the movement and load compensation PV is interesting. The load compensation PV is significantly distorted—elongated for lateral directions and biased away from the center for diagonal directions. This in itself is not surprising, as unit endpoint forces in lateral directions require higher joint torques (and thus higher muscle activation) as a result of the Jacobian transformation. The question is, why is the same effect not present in the movement PV? In the model, this results from the interplay of the F , M , B

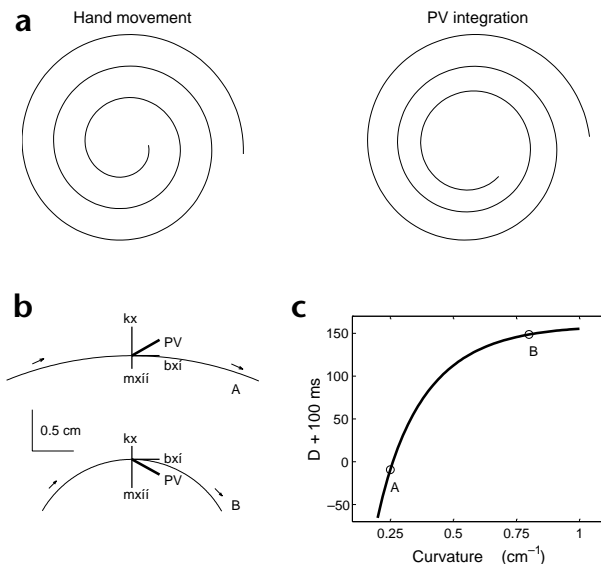


Fig. 4. Effects of curvature on PV direction. (a) Hand movement along a 1.5–7.5 cm spiral with a 2/3 power-law speed profile⁷ and its reconstruction by integrating the predicted PV over time. (b) Interplay among the three signals for different curvatures—for small curvature, PV direction lags behind tangential velocity, while for large curvature it leads. (c) Consider movements along circles with different radii R (locally approximating a spiral), with angular velocities⁷ well approximated by the 2/3 power law: $\omega = Ak^{2/3}$, where $\kappa = 1/R$ is curvature and $A \approx 12$ rad·cm per s. The hand trajectory is $x(t) = R \cos(\omega t)$, $y(t) = R \sin(\omega t)$. At $t = 0$ the tangent of the PV direction predicted by the model is $\frac{m\dot{\omega} - k\omega}{b}$ and the tangent of the instantaneous velocity is $\tan(\omega D)$. The solution $D = \text{atan}(\frac{m\dot{\omega} - k\omega}{b})/\omega$ is plotted, offset by a constant delay of 100 ms from cortical firing to force production. The two marked points correspond to the examples in (b).

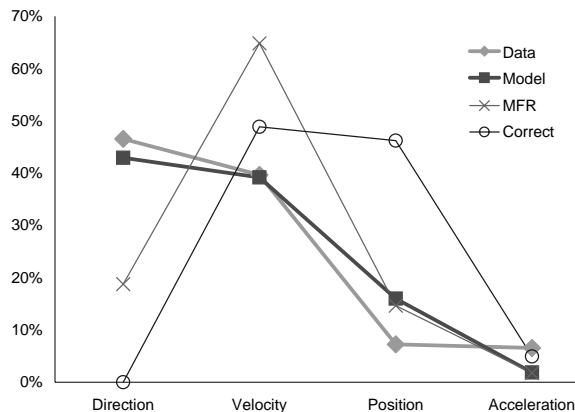


Fig. 5. Statistical biases in cell classification. The speed profile from Fig. 2 was scaled to match the hand kinematics shown in a previous study²¹. Movement extent, 0.15 m; peak velocity, 0.42 m per s; peak acceleration, 1.85 m per s². As previously²¹, movement start and end were defined as the times when the hand left a central 10-mm circle and entered a 35-mm target circle, respectively. Time-varying mean firing rates were generated from the model for 290 cells²¹. Each cell had a random PD and its own parameters c_i , k_i , b_i and m_i generated independently between 0 and twice the corresponding average values of $c = 8.5$, $k = 50$, $b = 10$, $m = 1$. The profiles were multiplied by 2; this together with the baseline of $c = 8.5$ scaled the population activity between 5 Hz (anti PD) and 45 Hz (PD) as in a previous study²⁷. Poisson spike trains were generated for five trials in each of eight directions with one-ms resolution and binned in ten-ms bins. The amount of smoothing (not given in ref. 21) was adjusted so that the median R^2 for the complete regression model matched the experimental value of 58%. The square root of the smoothed signal was defined as instantaneous activity²¹. For each cell, regressions of time-varying activity over all trials on direction, position, velocity and acceleration were performed separately, and the maximum R^2 was used to label the cell. The resulting percentages (model) are compared to experimental results²¹ (data). The same procedure was repeated with the underlying mfrs instead of spike data. The 'correct' percentages were also computed by separately averaging for each cell the absolute values of the three signals over time and trials and then finding the maximum. Here, 20 sets of 290 cells were generated and the averaged results plotted. STDs for all data points were less than 3%; that is, 290 cells are sufficient to obtain robust estimates.

and K ellipsoids (see Methods). Because they are all elongated in the same (y) direction, their effects tend to cancel during movement. The proportionality assumption makes them cancel exactly, that is, the constants m , b and k are the same in all directions. Although exact values of these matrices for monkeys remain to be measured experimentally, their general shape is derived from the geometry of the multijoint arm.

The PV can be computed in small time bins at different points along the movement, and its direction compared to the direction of movement. If the PV encodes movement velocity it should always point along the movement, if it encodes force + acceleration, its direction should reverse in the decelerating phase of the movement. Here the PV is a combination of both, so reversals should occur when the velocity term becomes smaller than the force + acceleration term (that is, when moving faster or adding a mass to the hand). Indeed, such reversals are seen²⁹ in experiments in which a monkey moves while holding the end of a pendulum. These reversals become even more common as the mass of the pendulum is increased and do not occur during isometric force¹⁰, in agreement with the model. Note that PV reversals are equivalent to the triphasic burst pattern (agonist–antagonist–agonist) described in EMG literature, which is most common during

rapid movements. Thus I would predict an increase of PV reversals if monkeys were trained to move faster.

Interestingly, PV reversals are seen mainly during lateral movements, although arm inertia is larger in the forward direction. Why should that be the case? Recall that reversals arise from additional isotropic mass (m_1) which has the effect of adding $m_1 F^{-1} \ddot{x}$ to the neural signal. Because F is elongated along the y axis, F^{-1} will be elongated along the x axis, thereby adding a larger force + acceleration signal in lateral directions.

Apparent fluctuations in MI-to-movement delay

Integrating the PV over time leads to a plausible reconstruction of hand paths⁷. Because the PV predicted by the model resembles movement velocity, integrating it leads to a similar reconstruction (Fig. 4). A more intriguing result suggests that the MI representation is time-varying, which would seem to contradict my model. Following this result, a time-varying delay $D(t)$ between MI firing and movement kinematics is defined in the following way: at each time step t , instantaneous PV direction is computed, and then the nearest time step $t + D(t)$ for which the direction of the tangential velocity is the same is found. The $D(t)$ computed in this way correlates with the curvature of the hand

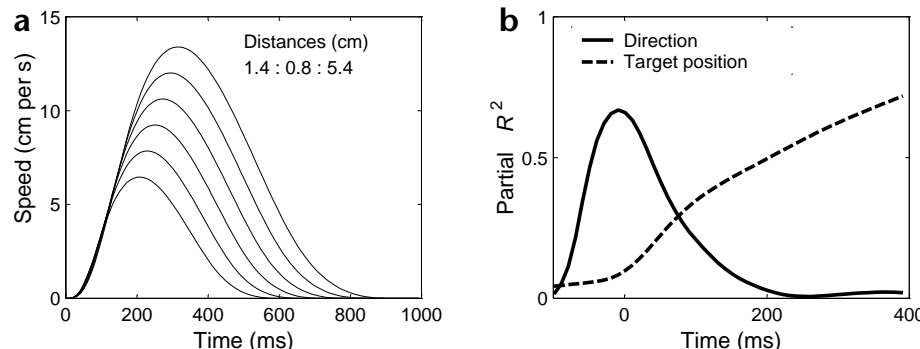


Fig. 6. Effects of kinematic scaling. (a) Skewed speed profiles in reaching at different distances, where peak velocity and movement duration scale with slopes 3 and 80 (in Hz, cm, ms) respectively⁵⁰. (b) Simulation of 100 cells with uniformly distributed PDs, and time-varying mean firing rates (mfr) computed from the model, with ± 1 Hz noise added in each 10-ms bin. Regression model at each time step t is: $mfr = a_0 + a_1 \cos\alpha + a_2 \sin\alpha + a_3 d \cos\alpha + a_4 d \sin\alpha$ where d is target distance and α is target direction. The partial R^2 between the mfr and 2D variable A is defined as the R^2 between A and the residual of the mfr regressed on B : $R_A^2 = R^2(mfr, A | B)$. A (B) are direction (target position) terms, and vice versa. Note that according to this definition, $R_{dir}^2 + R_{pos}^2 < R_{total}^2$ because of correlations between the target direction and position terms.

target direction. The partial R^2 between the mfr and 2D variable A is defined as the R^2 between A and the residual of the mfr regressed on B : $R_A^2 = R^2(mfr, A | B)$. A (B) are direction (target position) terms, and vice versa. Note that according to this definition, $R_{dir}^2 + R_{pos}^2 < R_{total}^2$ because of correlations between the target direction and position terms.

path⁷, being greater for large curvature and smaller (even negative) for small curvature (which implies that MI does not control but, instead, responds to parts of the movement).

This behavior is also observed in the model. The apparent fluctuations in $D(t)$ result from incorrectly treating the PV as a pure velocity signal⁷. The explanation is that for large curvature, the acceleration vector pointing inwards is large, advancing the PV direction relative to tangential velocity (Fig. 4). For small curvature and large movement radius, the acceleration vector is smaller and the position vector larger—yielding the opposite effect. A more precise analysis (Fig. 4) accounts quantitatively for three important features of the experimental data: $D(t)$ increases with curvature, the $D(t)$ curve is very steep for small curvatures and saturates for larger curvatures, and $D(t)$ can actually become negative. Thus the curvature-dependent changes in the MI-to-movement delay are observed only when $D(t)$ is computed using the instantaneous hand velocity, rather than the signal I propose.

Apparent significance of velocity/force direction

The remaining analyses are based on the model of individual cell responses in equation 2. Particularly important here are demonstrations of a significant contribution of velocity and force direction irrespective of magnitude^{21,30}. Such results would seem to contradict the model, which contains no explicit directional terms. The model successfully replicates those results, and clarifies what implicit assumptions and statistical biases cause the apparent contradiction.

For a center-out reaching task²¹, time-varying mean firing rates of individual neurons are regressed on four different sets of two-dimensional predictor variables: target direction (constant in each trial), measured hand position, velocity and acceleration. For each cell, the four separate regression models were compared and the cell was classified according to the model with highest R^2 value. Target-direction cells were most common (47%), suggesting that target direction was the most prominent factor underlying MI activity. The small percentage (6%) of hand-acceleration cells was used to argue against force-control models in general.

Surprisingly, replication of this analysis in detail on synthetic data²¹ (equation 2; Fig. 5) yields very similar results—target direction is again most prominent (43%), although the synthetic data is generated without any directional term. How is that possible? The first reason is a major statistical bias resulting from the smoothing of single-trial spike trains and taking the square root²¹. In the model, that step can be avoided by ‘observing’ the true mean firing rates instead of spike trains, and then applying identical analysis. That change is sufficient to decrease the percentage of target direction cells from 43% to 19%. But the direction cells still account for 19%, when a correct inference procedure should not find any. This is possible because the D, P, V and A waveforms used as predictor variables are correlated, and a linear combination of P, V and A can be more similar to D than any of its constituents. Thus, even with ‘ideal’ data, the prior assumption that direction cells exist is itself sufficient to bias the result of the analysis. Such biases raise the important question of how one can ever determine what an individual neuron controls²².

A related result comes from a three-dimensional isometric force study³⁰ that contrasted the contributions of force magnitude M and unit-length force direction vector X, Y, Z . Two regression models of cell firing d were compared: (D) $d = b_0 + b_x X + b_y Y + b_z Z$ and (M) $d = b_0 + b_m M$. Because only model (D) was significant in 79% of the tuned cells, it was concluded that force

direction, and not magnitude, is the most important determinant of MI firing.

To test whether the model replicates the results of this three-dimensional study, a similar two-dimensional analysis was applied to 300-ms Poisson spike trains for 150 synthetic cells, with firing rates scaled between 5 Hz (anti PD) and 50 Hz (PD), on 192 trials with different static forces³⁰. For roughly 90% of the synthetic cells only model (D) was significant at $p < 0.05$, and both models (D) and (M) were significant for the remaining 10% of cells. This is because the analysis implicitly assumes additive contributions of direction and magnitude: (D + M) $d = b_0 + b_x X + b_y Y + b_m M$. But the correct regression model for the synthetic data is a multiplicative one: (DM) $d = b_0 + b_{xm} XM + b_{ym} YM$. Indeed, model (DM) had a higher R^2 value (by 10% on average) than model (D + M) for each of the 150 synthetic cells, although it used one less parameter. Thus the original result may be due to a specific assumption regarding combination of the force direction and magnitude in the MI firing³⁰, which is violated in my model.

Apparent signal multiplexing

Another intriguing result indicates a temporal multiplexing of different signals in the MI population activity¹⁵, which would again seem to contradict the model. In a center-out reaching task with varying target direction (8) \times distance (6), the strength of partial correlations between MI activity and target direction is higher around movement onset; later, partial correlation is higher with target position, and even later, with target distance¹⁵. The first two results can be explained by applying the model to the hand kinematics inferred from this study¹⁵. The key is the following: in reaching to more distant targets, both the peak velocity and movement duration scaled up, in agreement with the speed-accuracy tradeoff known as Fitt’s law. As a result, the initial portions of the speed profile seem very similar across target distances (Fig. 6, left). Thus the MI encoding predicted by the model is best correlated with target direction around movement onset, and later becomes better correlated with target position (Fig. 6, right). An even later correlation with distance could be explained if cocontraction increased around the time of target acquisition³¹ in proportion to movement velocity.

This analysis leads to an important general point: the relative contributions of different movement parameters to MI firing are not invariant physiological characteristics, but depend on the details of motor behavior. To avoid reaching different conclusions about MI’s role whenever the monkey moves faster or holds an extra mass, the relative magnitudes of different kinematic and kinetic terms as observed in the task must be taken into account together, rather than normalized separately as they are in regression analyses.

DISCUSSION

In summary, I formulated a simple mechanistic model of force production which incorporates known properties of muscle physiology and multijoint mechanics. The model accounts for six main results. First, force magnitude is encoded in isometric tasks and velocity seems to be encoded in movement tasks; second, velocity is not encoded near the anti-preferred direction; third, directional PV is asymmetrical in force-related results but not in movement-related results; fourth, velocity and force direction seem to dominate without respect to magnitude; fifth, changes in MI-to-movement delay seem to be dependent on curvature, and sixth, direction and target position signals seem to be temporally multiplexed. At first glance, any one of these physiological find-

ings rules out earlier views of direct MI involvement in the control of muscle activation³. However, the contradictions can be traced to the incorrect implicit assumption that muscle activation alone determines endpoint force. In my model, most of these puzzling phenomena arise from the feedforward compensation of muscle viscoelasticity. Although realistic muscle properties are incorporated in one previous model of cortical control³², such compensation is not considered. A previously proposed additive model⁹ is related to equation 1, but all terms in it are interpreted as torque components—leaving the similarity to the velocity profile⁸ unexplained.

My model by no means provides a complete picture of MI into which all known pieces can fit. It is only a first approximation that attempts to solve as many puzzles as possible while assuming as little as possible. Clearly, equations 1 and 2 can only hold when MI and muscles are simultaneously active. For instance, in instructed-delay tasks, some form of gating at the level of the spinal cord must be assumed to explain how MI neurons can be active long before muscle activation.

Perhaps the most debated of the issues left out is that of reference frames. Studies that vary workspace location³³ or arm posture³⁴ yield changes of MI encoding consistent with a joint or muscle-based representation³⁵, in agreement with the model. A similar experiment with wrist movements³⁶ gives more mixed results—changes in preferred direction are consistent with both extrinsic and muscle-like encoding in different subpopulations. However, unlike a truly ‘extrinsic’ cell, most of the ‘extrinsic’ cells change their overall firing rate with posture. Such gain changes can be sufficient to maintain the consistency of equation 1 (which in itself implies no similarity between responses of individual cells and muscles). In particular, consider a muscle m driven by two cosine-tuned cells with gains $a_{1,2}$ and preferred directions $\mathbf{p}_{1,2}$. Omitting baselines, the muscle activity for force direction f is $m = a_1 f^T \mathbf{p}_1 + a_2 f^T \mathbf{p}_2 = f^T (a_1 \mathbf{p}_1 + a_2 \mathbf{p}_2)$, that is, the muscle is cosine-tuned with preferred direction $a_1 \mathbf{p}_1 + a_2 \mathbf{p}_2$. This vector can be rotated either by rotating $\mathbf{p}_{1,2}$ or by keeping $\mathbf{p}_{1,2}$ fixed and only varying $a_{1,2}$. To test whether this mechanism explains the results³⁶ would require knowledge of the ‘muscle fields’ of individual neurons, which could be recorded using spike-triggered EMG averaging⁵.

In isometric force tasks, the descending MI population activity is more phasic than EMG activity³⁷. This phenomenon may be entirely restricted to the onset of each trial, that is, an extra burst of activity may be required to overcome thresholds in the motor periphery. It is unlikely to encode an initial force transient³², because such a force transient is absent in isometric tasks³⁷. The few studies focusing on more prolonged behaviors fail to report any such effects in MI^{7,17} or the red nucleus³⁸ (another source of descending projections). Furthermore, the model is concerned only with pyramidal tract neurons, whose activity is less phasic than that of a mixed MI population⁹. If this initial phasic activity is indeed a transient ‘higher-order’ correction that does not reflect the underlying mode of MI control, it is better to omit it from the model at this stage. If future experiments indicate that the MI output is always more phasic than EMG activity, that is, some form of low-pass filtering takes place in the spinal interneurons, the term $Uc(t - \Delta)$ in equation 1 may have to be replaced by $\text{Filter}(Uc(t - \Delta))$. The low-pass filtering present in muscles^{24,25} can also be included. Then, to generate predictions about MI population activity, the right-hand side of equation 1 has to be unfiltered (deconvolved)—essentially adding terms proportional to its derivatives and making the prediction about $Uc(t - \Delta)$ more phasic.

The general model of central control deserves further discussion. It implicitly assumes that in the simple, overtrained, unperturbed movements studied here, feedforward central control can be quite accurate. Thus the limb will move very close to the reference point for activating spinal reflex loops, minimizing their contribution to muscle activity. This model assumption is similar to the conclusions of psychophysical studies³⁹, as well as robotic-control algorithms motivated by computational efficiency and manipulator stability⁴⁰. If this assumption turns out to be incorrect and reflexes always contribute significantly to muscle activity, their gains could be added to the corresponding impedance terms in the present formulation. Similarly, descending projections from the red nucleus could be included in the vector $c(t - \Delta)$ —in agreement with experimental observations³⁸.

METHODS

Notation. x is a scalar, \mathbf{x} is a column vector and \mathbf{x}^T is a transposed (row) vector. Thus $\mathbf{x}^T \mathbf{y}$ is the dot product of \mathbf{x} and \mathbf{y} , X is a matrix, $\text{Diag}(\mathbf{x})$ is the diagonal matrix with vector \mathbf{x} along the main diagonal, $\lfloor \mathbf{x} \rfloor$ returns \mathbf{x} for positive numbers and 0 otherwise, $\dot{\mathbf{x}}$ and $\ddot{\mathbf{x}}$ are temporal derivatives of \mathbf{x} , $|X|$ is a determinant, and X^{-1} is a matrix inverse.

Model formulation. The muscle activations a_i are modeled as time-delayed sums of MI pyramidal tract activities c_i multiplied by synaptic weights w_{ij} ; in vector notation, $\mathbf{a}(t) = Wc(t - \Delta)$. A similar linear summation model captures the relationship between EMG and red nucleus activity³⁸. Comparisons of onset time and activation magnitude between MI and EMG⁴¹ support such a direct activation model. Also, the effects of simultaneous microstimulations add linearly—both in terms of endpoint force fields⁴² and EMG activity⁴³.

The mechanisms of muscle force production have been well characterized, both on the microscopic and macroscopic levels^{24,25}. For fixed activation a , muscle force f varies with length l and velocity \dot{l} (l increases in the direction of shortening). The effect of velocity (damping) is asymmetric; it is predominantly present during shortening²³. The first-order model $f(a, l, \dot{l}) = a - kl - \lfloor b \dot{l} \rfloor$ provides a reasonable approximation²⁵ (a is assumed large enough to prevent f from being negative).

The direction of hand movement for which a muscle shortens most rapidly is very close to the direction in which it produces endpoint force, and its orientation varies little over a small workspace (Fig. 1). Thus the position- and velocity-dependent endpoint-force field $f_i(a_i, \mathbf{x}, \dot{\mathbf{x}})$ that muscle i generates can be summarized by a ‘muscle force vector’ \mathbf{p}_i and the coefficients k_i , b_i :

$$f_i = p_i (a_i - b_i \lfloor p_i^T \dot{\mathbf{x}} \rfloor - k_i p_i^T \mathbf{x})$$

The workspace is centered at 0. The arm is modeled as anisotropic point mass in endpoint space with inertia matrix M , the force exerted against external objects is \mathbf{f} , and all p_i s are assembled in the columns of the matrix P . The distribution of force directions \mathbf{p}_i can be arbitrary. Adding the forces generated by all muscles and using Newton’s second law yields

$$P(Wc(t - \Delta) - \text{Diag}(\mathbf{b}(\dot{\mathbf{x}}))P^T \dot{\mathbf{x}}(t) - \text{Diag}(\mathbf{k})P^T \mathbf{x}(t)) = \mathbf{f}(t) + M\ddot{\mathbf{x}}(t)$$

where the i th element of vector $\mathbf{b}(\dot{\mathbf{x}})$ is b_i when $p_i^T \dot{\mathbf{x}} > 0$, and 0 otherwise. Assuming that system-level stiffness and damping are dominated by muscle (rather than passive, joint) properties, the endpoint stiffness and damping matrices are $K = P \text{Diag}(\mathbf{k})P^T$ and $B = P \text{Diag}(\mathbf{b}(\dot{\mathbf{x}}))P^T$. Expanding the brackets and moving the impedance terms to the right hand side, the constraint on $c(t - \Delta)$ becomes

$$P W c(t - \Delta) = \mathbf{f}(t) + M\ddot{\mathbf{x}}(t) + B\dot{\mathbf{x}}(t) + K\mathbf{x}(t) \quad (4)$$

Because experimental measurements of M , B and K in monkeys are not available, I use approximate values for the human arm, which are probably scaled-up versions²⁴. I assume that synaptic weights W onto muscles, and joint torque magnitudes for unit muscle activation do not vary

systematically with endpoint force direction. Thus the only anisotropy in PW results from multijoint mechanics; that is, the magnitudes of the column vectors in the matrix PW will be larger along the hand–shoulder (y) axis because of the Jacobian transformation. Then PW can be approximated by $F_{2 \times 2} U_{2 \times \text{Cells}}$, where the columns of U are unit length vectors and F is a ‘force matrix’ that stretches column vectors from U pointing along the y axis. Other possible sources of anisotropy can also be absorbed in F . The ellipsoids corresponding to M , B and K are also elongated along the y axis^{44,45}; this holds for M , as the elbow points downward in typical center-out reaching tasks. As all four ellipsoids have similar orientations and aspect ratios, it will be assumed for simplicity that they are proportional to each other: $M = mF$, $B = bF$, $K = kF$, $|F| = 1$. Then equation 4 can be rewritten as equation 1. A strictly causal model must explain how the motor system ‘knows’ what the behavior $f(t)$, $\ddot{x}(t)$, $\dot{x}(t)$, $x(t)$ will be after a delay Δ to generate the MI output $c(t - \Delta)$. One possibility which is particularly attractive from a control point of view⁴⁰ is that $f(t)$, $\ddot{x}(t)$ are set to desired external force and acceleration, whereas $\dot{x}(t)$, $x(t)$ are set to predicted velocity and position. Such predictions could be obtained from a Kalman-like filter⁴⁶—using delayed sensory feedback, an efference copy of recent motor commands and a forward model of the motor periphery.

Joint space formulation. I have adopted an endpoint formulation, because MI data is traditionally presented in endpoint space and joint angles not even recorded (the differences over a small workspace are likely to be minimal⁴⁷). The formulation of the model in joint space is very similar. Using a local linearization, $B_\theta = J^T B_x J$ and $\dot{x} = J\theta$, so $B_\theta \dot{\theta} = J^T B_x \dot{x}$ (similarly for the \ddot{x} and x terms). The joint space equivalent of equation 1 is

$$Tc = J^T(f + M_x \ddot{x} + B_x \dot{x} + K_x x) + g(\theta, \dot{\theta})$$

where the matrix of cell-torque directions T replaces U , g is a Coriolis term, and the Jacobian J^T replaces F^{-1} . Thus F^{-1} is well defined even in the case of mechanical redundancy.

Optimality of cosine tuning. Consider a continuous family of isometric force generators indexed by $\alpha \in [0; 2\pi]$ with activation levels $c(\alpha) \in R$ and unit force directions $u(\alpha) \in R^2$. Each generator contributes force $(c(\alpha) + z(\alpha))u(\alpha)$, where $z(\alpha)$ are independent random variables (neuromotor noise) with $\text{Var}(z(\alpha)) = c(\alpha)^2$ as observed experimentally⁴⁸. Then the net force is $w = \int(c(\alpha) + z(\alpha))u(\alpha)d\alpha$. What activation profile $c(\alpha)$ minimizes $\text{Var}(w) = \int c(\alpha)^2$ for specified mean force $r = \int c(\alpha)u(\alpha)d\alpha$ and specified $C = \int c(\alpha)d\alpha$ coactivation? From Parseval’s theorem $\int c(\alpha)^2 = a_0^2 + \sum_{k=1}^{\infty} a_k^2 + b_k^2$, where a_0, a_1, b_1, \dots are the Fourier series coefficients of $c(\alpha)$. The constraints given by r, C fix the values of a_0, a_1 and b_1 , so the infinite sum is minimized when all other terms are 0. Thus a cosine centered on the specified force direction is the optimal activation profile that minimizes expected error but achieves (on average) the specified force and coactivation.

ACKNOWLEDGEMENTS

I thank Zoubin Ghahramani and Stephen Scott for their suggestions.

RECEIVED 21 SEPTEMBER 1999; ACCEPTED 15 FEBRUARY 2000

1. Evarts, E. V. in *Handbook of Physiology* (ed. Brooks, V. B.) 1083–1120 (Williams and Wilkins, Baltimore, 1981).
2. Johnson, P. B. in *Control of Arm Movement in Space: Neurophysiological and Computational Approaches* (eds. Caminiti, R., Johnson, P. B. & Burnod, Y.) (Springer, Berlin, 1992).
3. Evarts, E. Relation of pyramidal tract activity to force exerted during voluntary movement. *J. Neurophysiol.* **31**, 14–27 (1968).
4. Dum, R. P. & Strick, P. L. The origin of corticospinal projections from the premotor areas in the frontal lobe. *J. Neurosci.* **11**, 667–669 (1991).
5. Fetz, E. E. & Cheney, P. D. Postspike facilitation of forelimb muscle activity by primate corticomotoneuronal cells. *J. Neurophysiol.* **44**, 751–772 (1980).
6. Georgopoulos, A., Kalaska, J., Caminiti, R. & Massey, J. On the relations between the direction of two-dimensional arm movements and cell discharge in primate motor cortex. *J. Neurosci.* **2**, 1527–1537 (1982).
7. Schwartz, A. B. Direct cortical representation of drawing. *Science* **265**, 540–542 (1994).
8. Moran, D. W. & Schwartz, A. B. Motor cortical representation of speed and direction during reaching. *J. Neurophysiol.* **82**, 2676–2692 (1999).
9. Kalaska, J. F., Cohen, D. A. D., Hyde, M. L. & Prud’homme, M. A comparison of movement direction-related versus load direction-related activity in primate motor cortex, using a two-dimensional reaching task. *J. Neurosci.* **9**, 2080–2102 (1989).
10. Sergio, L. E. & Kalaska, J. F. Changes in the temporal pattern of primary motor cortex activity in a directional isometric force versus limb movement task. *J. Neurophysiol.* **80**, 1577–1583 (1998).
11. Kettner, R. E., Schwartz, A. B. & Georgopoulos, A. P. Primate motor cortex and free arm movements to visual targets in three-dimensional space III. Positional gradients and population coding of movement direction from various movement origins. *J. Neurosci.* **8**, 2938–2947 (1988).
12. Flament, D. & Hore, J. Relations of motor cortex neural discharge to kinematics of passive and active elbow movements in the monkey. *J. Neurophysiol.* **60**, 1268–1284 (1988).
13. Thach, W. T. Correlation of neural discharge with pattern and force of muscular activity, joint position, and direction of intended next movement in motor cortex and cerebellum. *J. Neurophysiol.* **41**, 654–676 (1978).
14. Alexander, G. E. & Crutcher, M. D. Neural representations of the target (goal) of visually guided arm movements in three motor areas of the monkey. *J. Neurophysiol.* **64**, 164–178 (1990).
15. Fu, Q.-G., Flament, D., Coltz, J. D. & Ebner, T. J. Temporal encoding of movement kinematics in the discharge of primate primary motor and premotor neurons. *J. Neurophysiol.* **73**, 836–854 (1995).
16. Hocherman, S. & Wise, S. P. Effects of hand movement path on motor cortical activity in awake, behaving rhesus monkeys. *Exp. Brain Res.* **83**, 285–302 (1991).
17. Humphrey, D. R. & Reed, D. J. in *Advances in Neurology: Motor Control Mechanisms in Health and Disease* (ed. Desmedt, J. E.) 347–372 (Raven, New York, 1983).
18. Carpenter, A. F., Georgopoulos, A. P. & Pellizzetti, G. Motor cortical encoding of serial order in a context-recall task. *Science* **283**, 1752–1757 (1999).
19. Georgopoulos, A. P., Lurito, J. T., Petrides, M., Schwartz, A. B. & Massey, J. T. Mental rotation of the neuronal population vector. *Science* **243**, 234–236 (1989).
20. Scott, S. & Kalaska, J. Changes in motor cortex activity during reaching movements with similar hand paths but different arm postures. *J. Neurophysiol.* **73**, 2563–2567 (1995).
21. Ashe, J. & Georgopoulos, A. P. Movement parameters and neural activity in motor cortex and Area 5. *Cereb. Cortex* **6**, 590–600 (1994).
22. Fetz, E. E. Are movement parameters recognizably coded in the activity of single neurons? *Behav. Brain Sci.* **15**, 679–690 (1992).
23. Joyce, G. C., Rack, P. M. H. & Westbury, D. R. The mechanical properties of cat soleus muscle during controlled lengthening and shortening movements. *J. Physiol. (Lond.)* **204**, 461–474 (1969).
24. Zajac, F. E. Muscle and tendon: properties, models, scaling, and application to biomechanics and motor control. *Crit. Rev. Biomed. Eng.* **17**, 359–411 (1989).
25. Winter, D. A. *Bio mechanics and Motor Control of Human Movement* (Wiley, New York, 1990).
26. Hubel, D. H. & Wiesel, T. N. Receptive fields, binocular interaction and functional architecture in the cat’s visual cortex. *J. Physiol. (Lond.)* **160**, 106–154 (1962).
27. Crammond, D. J. & Kalaska, J. F. Differential relation of discharge in primary motor cortex and premotor cortex to movements versus actively maintained postures during a reaching task. *Exp. Brain Res.* **108**, 45–61 (1996).
28. Kalaska, J. F. & Crammond, D. J. Cerebral cortical mechanisms of reaching movements. *Science* **255**, 1517–1523 (1992).
29. Kalaska, J. F., Crammond, D. J., Cohen, D. A. D., Prud’homme, M. & Hyde, M. L. in *Control of Arm Movement in Space: Neurophysiological and Computational Approaches* (eds. Caminiti, R., Johnson, P. B. & Burnod, Y.) (Springer, Berlin, 1992).
30. Taira, M., Boline, J., Smyrnis, N., Georgopoulos, A. & Ashe, J. On the relations between single cell activity in the motor cortex and the direction and magnitude of three-dimensional static isometric force. *Exp. Brain Res.* **109**, 367–376 (1996).
31. Bennett, D. J., Hollerbach, J. M., Xu, Y. & Hunter, I. W. Time-varying stiffness of human elbow joint during cyclic voluntary movement. *Exp. Brain Res.* **88**, 433–442 (1992).
32. Bullock, D., Cisek, P. & Grossberg, S. Cortical networks for control of voluntary arm movements under variable force conditions. *Cereb. Cortex* **8**, 48–62 (1998).
33. Caminiti, R., Johnson, P. & Urbano, A. Making arm movements within different parts of space: dynamic aspects in the primate motor cortex. *J. Neurosci.* **10**, 2039–2058 (1990).
34. Scott, S. & Kalaska, J. Reaching movements with similar hand paths but different arm orientation. I. Activity of individual cells in motor cortex. *J. Neurophysiol.* **77**, 826–852 (1997).
35. Tanaka, S. Hypothetical joint-related coordinate systems in which populations of motor cortical neurons code direction of voluntary arm movements. *Neurosci. Lett.* **180**, 83–86 (1994).

articles

36. Kakei, S., Hoffman, D. & Strick, P. Muscle and movement representations in the primary motor cortex. *Science* **285**, 2136–2139 (1999).
37. Fetz, E. E., Cheney, P. D., Mewes, K. & Palmer, S. Control of forelimb muscle activity by populations of corticomotoneuronal and rubromotoneuronal cells. *Prog. Brain Res.* **80**, 437–449 (1989).
38. Miller, L. E. & Sinkjaer, T. Primate red nucleus discharge encodes the dynamics of limb muscle activity. *J. Neurophysiol.* **80**, 59–70 (1998).
39. Gottlieb, G. L. On the voluntary movement of compliant (inertial-viscoelastic) loads by parcellated control mechanisms. *J. Neurophysiol.* **76**, 3207–3228 (1996).
40. Khatib, O. A unified approach to motion and force control of robotic manipulators: the operational space formulation. *IEEE J. Robotics Automat.* **RA-3**, 43–53 (1987).
41. Scott, S. H. Comparison of onset time and magnitude of activity for proximal arm muscles and motor cortical cells before reaching movements. *J. Neurophysiol.* **77**, 1016–1022 (1997).
42. Bizzzi, E., Mussa-Ivaldi, F. A. & Giszter, S. F. Computations underlying the execution of movement: a biological perspective. *Science* **253**, 287–291 (1991).
43. Galagan, J. Spinal Mechanisms of Motor Control. Thesis, MIT (1999).
44. Tsuij, T., Morasso, P. G., Goto, K. & Ito, K. Human hand impedance characteristics during maintained posture. *Biol. Cybern.* **72**, 475–485 (1995).
45. Gomi, H. & Kawato, M. Equilibrium-point control hypothesis examined by measured arm stiffness during multijoint movement. *Nature* **272**, 117–120 (1996).
46. Wolpert, D., Gharahmani, Z. & Jordan, M. An internal model for sensorimotor integration. *Science* **269**, 1880–1882 (1995).
47. Mussa-Ivaldi, F. A. Do neurons in the motor cortex encode movement direction? An alternative hypothesis. *Neurosci. Lett.* **91**, 106–111 (1988).
48. Schmidt, R. A., Zelaznik, H., Hawkins, B., Frank, J. S. & Quinn, J. T. J. Motor-output variability: a theory for the accuracy of rapid motor acts. *Psychol. Rev.* **86**, 415–451 (1979).
49. Sanes, J. N. & Shadmehr, R. Sense of muscular effort and somesthetic afferent information in humans. *Can. J. Physiol. Pharmacol.* **73**, 223–233 (1995).
50. Fu, Q.-G., Suarez, J. & Ebner, T. Neuronal specification of direction and distance during reaching movements in the superior precentral premotor area and primary motor cortex of monkeys. *J. Neurophysiol.* **70**, 2097–2116 (1993).